Low-power, small-size transmitter module with metamaterial antenna

Kazuki Hiraishi*, Toshiki Wada*, Keishi Kubo*, Yutaro Otsu*, Masayuki Ikebe†, and Eiichi Sano*

*Research Center for Integrated Quantum Electronics, Hokkaido University, Sapporo 060–8628 Japan

†Graduate School of Information Science and Technology, Hokkaido University, Sapporo 060–0814 Japan

Tel: +81-11-706-7174, Fax: +81-11-706-6004

E-mail: esano@rciqe.hokudai.ac.jp

Abstract— Development of a low-power, small-size transmitter is needed for wireless sensor networks. An effective way to reduce power consumption is to reduce the operating time in a voltage-controlled oscillator. In this study, a 2.4 GHz on-off keying (OOK) transmitter circuit is designed and implemented with an electrically small antenna using a left-handed transmission line. The transmitter circuit was fabricated with a standard 0.18 μm CMOS technology, while the antenna was fabricated with a 3.0×4.5 cm printed circuit board, chip capacitors, and chip inductors. Measured output power was -6.8 dBm with a power consumption of 3.59 mW when the baseband signal was always “high”. The power consumption was reduced to 1.96 mW for the baseband signal with a mark ratio of 0.5.

Keywords: OOK, VCO, low-power, metamaterial, 2.4GHz, sensor network

1. Introduction

Recent years have seen the development of wireless sensor networks (WSNs) to realize ubiquitous computing environments. A WSN is a network to get information from wireless sensor nodes located at distant sites. Today, WSNs are used in various fields such as building and apartment security and healthcare monitoring. Small size and low power consumption is needed for wireless sensor nodes to be deployed and to ensure maintenance-free operation in various environments since it is difficult to constantly maintain a huge number of sensor nodes in a manner like that of replacing batteries [1].

The size of a wireless sensor node is mainly determined by antenna size. In recent years, several extensive attempts have been made to fabricate electrically small antennas for system-on-a-chip (SoC) or system-in-a-package (SiP) application [2], [3]. However, in such antennas the antenna gain is constrained to the Harrington limit, while the impedance matching and directivity characteristics deteriorate. Various methods for reducing antenna size have been reported [3-8]. Using a dipole antenna loaded with a left-handed ladder structure is a promising technique for reducing the size of antennas [5]. When parallel plate capacitors and spiral inductors are fabricated on a printed circuit board (PCB) with a thickness of a few mm, however, the sizes of the capacitors and the widths of the spiral inductors are expected to be more than 4 × 4 mm and 2 mm for achieving left-handed components operating at 2.4 GHz, and these components cannot reduce the antenna size to less than a conventional dipole antenna. In contrast, lumped components of inductors and capacitors with sizes of 0.4 × 0.2 and 0.6 × 0.3 mm are commercially available.

In this paper, a 2.4 GHz on-off keying (OOK) transmitter circuit, one of the key components in wireless sensor nodes, was designed and fabricated with a 0.18 μm CMOS technology. To reduce the power consumption, a merged configuration of a voltage controlled oscillator (VCO) and a mixer was adopted. The fabricated CMOS IC was implemented on a PCB with an electrically small antenna using a left-handed transmission line [9].

2. Transmitter

2.1 Circuit configuration

We assumed a simple modulation scheme such as OOK or pulse width modulation (PWM) [1] for low bit rate sensor applications. In general, a transmitter consists of a VCO, mixer, and power amplifier (PA). To reduce the operating time and the power consumption of the VCO, the mixer was merged with the VCO in our circuit. Figure 1 shows a schematic of the proposed transmitter circuit. When the baseband signal is “1”, the NMOS transistor M7 is turned on and the PMOS transistors M1 and M4 are turned off. Accordingly, the circuit acts as an *LC*-VCO composed of the transistors (M2, M3, M5, and M6), inductor,

and varactors, which results in the generation of a carrier wave. On the other hand, when the baseband signal is “0”, forcing the PMOS transistors M1 and M4 to turn on, V_{out} is equal to V_{dd} and the oscillation halts. This leads to reductions in the power consumption of the VCO and the fall time of the RF signal modulated by the baseband signal. The output port of the mixer/VCO is connected to the input port of the PA. A class-D configuration was used to increase the power-added efficiency. An impedance matching circuit consisting of a capacitor and an inductor was introduced at the output port. The parasitic elements, associated with the bonding pad and the wire, were taken into account in the design.

2.2 Simulation results

We designed the transmitter in a TSMC (Taiwan Semiconductor Manufacturing Co., Ltd.) 0.18-μm mixed signal/RF CMOS process with one poly and six metal layers by using a circuit simulator (Agilent ADS and Cadence Virtuoso). Table 1 summarizes the device sizes in the transmitter circuit. Here, W is the gate width of the MOSFET, W_{ind} is the width of the inductor, R is the inner radius of the inductor, N_{ind} is the number of turns of the inductor, W_{var} is the width of each varactor finger, and N_{var} is the number of varactor fingers. All the gate lengths of the MOSFETs were 0.18 μm.

Figure 2 shows the simulated output waveform of the transmitter with V_{dd} of 1.5 V and a varactor control voltage of 0.75 V when modulated by a 40 Mb/s “10101010” NRZ baseband signal. The simulated peak-to-peak voltage of the output waveform was 560 mV with 2.1 mW power consumption. The simulated power consumptions were 0.45 mW and 1.64 mW for the mixer/VCO and PA, respectively. The fall time was 2 ns while the rise time was 5 ns, which clearly demonstrated the effect of the PMOS transistors M1 and M4. The phase noise of the VCO was -119.47 Hz/dBc at 1 MHz offset. The output impedance of the VCO was 104.46-j25.50 Ω at 2.45 GHz. The conversion gain was -6.43 dB.

Figure 3 shows the simulated power spectrum for the transmitter with a power consumption of 4.2 mW when the baseband signal is kept constant at “1”. Output power was -1.4 dBm at 2.465 GHz. The power-added efficiency (PAE), gain, and input impedance of the designed PA were 15 %, 2.2 dB, and 26.5-j321.43 Ω at 2.45 GHz, respectively.

The impedance matching between the mixer/VCO and PA was not particularly good. We designed buffer circuits and impedance matching circuits between them. According to the design, the optimized buffer circuits were constructed with four-stage inverters, which resulted in increased power consumption. However, the *LC* matching circuits did not increase the input power into the PA due to the parasitic resistances in the spiral inductor and MIM capacitor. Therefore, the mixer/VCO was connected directly to the PA.

Figure 4 shows the simulated circuit performance, taking into account variations in fabrication procedure and ambient temperature when the baseband signal is kept constant at “1”. A faster MOSFET increased the output power and power consumption. Elevated temperature decreased the output power

and power consumption. While the transmitter efficiency was 18.7% for typical/typical MOSFETs at 25 degree C, it was 22.6% for faster/faster MOSFETs at 0 degree C and 12.7% for slower/slower MOSFETs at 70 degree C.

3. Antenna design

The length for a standard half-wavelength dipole antenna operating at 2.4 GHz is about 6 cm, which is too long to achieve a small-size sensor node. On the other hand, we encounter a problem that the antenna gain degrades as the antenna size is reduced. The highest achievable gain of an electrically small antenna that can be enclosed within a sphere of effective radius r is given by

$$\mathrm{G} = (kr)^2 + 2kr \tag{1}$$

where k is the wave number.

Various methods have been proposed for aiming at the gain limit of the small antennas given by (1). In this work, we use a metamaterial antenna using left-handed elements [9], [10]. The configuration of the composite right-/left-handed dipole antenna is shown in Fig. 5(a). Shunt inductors and series capacitors as left-handed elements are inserted in the right-handed transmission line. The dispersion characteristics for a right-handed transmission line are described by the propagation constant

$$\gamma = \alpha + \mathrm{j}\beta, \tag{2}$$

where α is the attenuation constant and β is the phase constant. In a lossless case, β is given by

$$\gamma = \mathrm{j}\beta = \sqrt{j\omega L \cdot j\omega C} = j\omega\sqrt{LC}, \tag{3}$$

where L is the inductance and C is the capacitance. This equation indicates that β is proportional to the angular frequency ω. The use of a series capacitor and a shunt inductor enable a left-handed transmission line to be fabricated. In the lossless case, the propagation constant for the left-handed transmission line is given by

$$\gamma = j\beta = \sqrt{\frac{1}{j\omega C} \cdot \frac{1}{j\omega L}} = \frac{1}{j\omega}\sqrt{\frac{1}{LC}}, \tag{4}$$

which indicates that β is inversely proportional to ω. This property is used for achieving a small antenna.

In practice, a pure left-handed transmission line cannot be fabricated because of parasitic inductances and capacitances. The propagation constant including the parasitic components is given by [10]

$$\gamma = \sqrt{ZY} = js(\omega)\sqrt{\omega^2 L_R C_R + \frac{1}{\omega^2 L_L C_L} - \frac{1}{L_L C_L}\left(\frac{1}{\omega_{se}{}^2} + \frac{1}{\omega_{sh}{}^2}\right)}, \tag{5}$$

where L_L and C_L are the left-handed elements and L_R and C_R are the right-handed components. The series and parallel resonating frequencies ω_{se} and ω_{sh} are given by

$$\omega_{se} = \frac{1}{\sqrt{L_R C_L}}, \tag{6}$$

and

$$\omega_{sh} = \frac{1}{L_L C_R}, \tag{7}$$

In (5), $s(\omega)$ is given by

$$s(\omega) = \begin{cases} -1 \; if \; \omega < \min(\omega_{se}, \omega_{sh}) \\ +1 \; if \; \omega > \max(\omega_{se}, \omega_{sh}) \end{cases}, \tag{8}$$

where $s(\omega)$ = -1for the left-handed branch and $s(\omega)$ = 1 for the right-handed branch. A periodic boundary condition leads to

$$\beta p = \cos^{-1}\left[1 - \frac{1}{2}\left(\omega L_R - \frac{1}{\omega C_L}\right)\left(\omega C_R - \frac{1}{\omega L_L}\right)\right]. \tag{10}$$

where p is the length of a unit cell. The L_R and C_R for the two parallel lines are given by

$$L_R = \frac{p\mu_0}{\pi} \ln\left(\frac{H}{R}\right) \tag{11}$$

$$C_R = \frac{\pi p \varepsilon_0 \varepsilon_r}{\ln \frac{H}{R}} \tag{12}$$

where H is the distance between the parallel lines and R is the half line width [6]. Since both ends of the lines open, the amount of phase change between the two open ends must be π at the target frequency of 2.4 GHz. This means that βp must equal π/4 in the 4-cell configuration.

The designed values were: p=5 mm, H=2 mm, R=0.3 mm, C_L=0.5 pF, L_L=3.9 nH. Since the output of the transmitter was single-ended, the T-junction balun shown in Fig. 5(b) was inserted between the antenna and the transmitter.

4. Measurement results

4.1 Transmitter IC

We fabricated the transmitter using the TSMC 0.18-μm mixed signal/RF CMOS process. Figure 6 shows a photograph of the fabricated transmitter IC which was 1.3 × 0.8 mm^2 in size. The transmitter IC was mounted on a PCB with a commercially available fine coaxial connector. The output characteristics for the transmitter IC were evaluated using a spectrum analyzer and an oscilloscope. The measurements were performed at room temperature and the temperature dependence of the performance was not measured. The measured oscillation frequency for the VCO covered 2.270–2.544 GHz when the varactor control voltage V_{ctrl} was varied from 0 to 1.5 V. Figure 7 shows the measured output waveform of the transmitter with V_{dd}=1.5 V and V_{ctrl}=0.9 V when the baseband signal of 100 kHz repetition pulses were input. An OOK RF signal with a peak-to-peak voltage larger than 320 mV was successfully obtained. Figure 8 shows the output power spectrum of the transmitter IC with V_{ctrl}=0.9 V. The output power was -4.56 dBm at 2.42 GHz and the power consumption was 1.96 mW. The measured output power was 3 dB lower than the simulated value. The difference might be mainly caused by the losses of the signal line on the PCB,

the fine coaxial connector, and the cable used in the measurements. Figure 9 shows the measured and simulated return loss characteristics of the output when the baseband signal was maintained at 0 V. The agreement between the simulated and measured return loss at around 2.9 GHz was good. The reason for the discrepancy at 3.9 and 4.8 GHz is still unclear.

4.2 Antenna

Figure 10 shows a photograph of the antenna and balun fabricated with commercially available chip capacitors and inductors with a size of 0.6 × 0.3 mm on an FR4 substrate with a thickness of 1.6 mm and the experimental setup used for characterizing the radiation pattern and gain of the antenna. The fabricated antenna was measured using a standard dipole antenna with a gain of 2.4 dBi and a VNA. The gain was calibrated with the gain measured between two standard dipole antennas. The effect of a connector and cable nearby the antenna was negligibly small (See Electronic Supplementary Material). Figure 11 shows the measured return loss characteristics with the simulation results. The matching between designed and measured return losses was quite good. Figure 12 shows the measured antenna gain with error bars for three antennas. The measured antenna gain at 2.45 GHz was -0.01 dBi. The simulated gain (-0.66 dBi) was slightly lower; the difference might have been caused by the variation in the lumped elements and the effect of the solder used to mount the components. The measured variation in the lumped elements ranged from -3% to +6%, which caused deviations in the simulated antenna gain of less than 1 dB. Although the temperature dependence of the antenna gain was not measured, the simulations indicated that the deviation in the antenna gain was less than 0.1 dB for 0-75 degree C range. Therefore, the effect of production and temperature variations was negligibly small. Figure 13 compares measured and simulated directivities, for which good agreement was obtained. Figure 14 compares the antenna gain achieved in this work with those reported in previous literature [3]-[5], [7], [8]. The former was about 1 dB lower than the Harrington limit.

4.3 Transmitter module

A transmitter module was assembled with the transmitter IC and the metamaterial antenna. Figure 15 shows the experimental setup of the transmitter. A battery in an electromagnetic shield was used to generate V_{ctrl} to reduce the power supply noise. Figure 16 shows the power spectrum received by a standard dipole antenna located 30 cm from the transmitter module in the CW operation with V_{ctrl}=1.06 V (adjusted to generate a 2.45 GHz carrier wave). After calibrating the cable loss and the propagation loss in free space, the output power from the module was -6.8 dBm. This value was about 2 dB smaller than the value calculated from the output power of the transmitter IC and the antenna gain. The reduction might be caused by the gain difference between the individual antenna described in 4.2 and the antenna in the

module. As can be seen from Figure 10, the transmission lines in the individual antenna were coated with thick solder; those in the module were coated with resin. This might cause the differences in the loss and the parameters in the right-handed transmission line (C_R and L_R). The power consumption was 3.59 mW.

Finally, we measured the output waveform from the module modulated with a 100 kHz baseband signal. Figure 17 shows the waveform received by the standard dipole antenna. An OOK RF signal was successfully obtained with a power consumption of 1.96 mW. We measured two transmitter modules. The difference in power consumption between the two was 0.1 mW under the condition that the transmitters had the same output power. Table 2 compares the performance of our transmitter with four OOK transmitters previously measured in the literature. The power consumption of the transmitter reported in [11] was higher than ours because the oscillator was always operating. Although the transmitter reported in [12] achieved higher efficiency by using 90-nm CMOS processes, the circuit configuration had lower efficiency than ours because the oscillator was always operating. Although the transmitter reported in [13] had the same modulation scheme as ours, it achieved lower efficiency because it had no PA. Moreover, the transmitter was fabricated by using an off-chip inductor. The transmitter reported in [14] had higher efficiency than ours due to its use of an off-chip high Q film bulk acoustic resonator. It is clear from the table that our transmitter achieved the highest power efficiency of the transmitters using 0.18-μm CMOS processes.

5. Conclusion

We designed and fabricated a 2.4 GHz low-power, small-size transmitter module. A merged mixer/VCO configuration and a class-D power amplifier were used to reduce the power consumption. A metamaterial design technique was introduced to achieve an electrically small antenna with a sufficient gain. The output power of the fabricated transmitter module in the CW operation was -6.8 dBm with a power consumption of 3.59 mW. The power consumption was reduced to 1.96 mW when the RF signal as modulated with the baseband signal. Table 2 compares the performance of our transmitter with eight transmitters previously measured in the literature. The present design method will be useful for achieving low-power, small-size wireless sensor nodes.

Acknowledgments

This work was partially supported by SCOPE, and by VDEC in collaboration with Cadence Design Systems, Inc., and Agilent Technologies Japan, Ltd.

References

1. Takahagi, K., Matsushita, H., Iida, T., Ikebe, M., Amemiya, Y., & Sano, E. (2013). Low-power wake-up receiver with subthreshold CMOS circuits for wireless sensor networks. *Analog Integrated Circuits and Signal Processing*, *75*, 199-205.

2. Takahagi, K. & Sano, E. (2011). High-gain silicon on-chip antenna with artificial dielectric layer. *IEEE Transactions on Antennas and Propagation*, 59(10), 3624-3629.

3. Chi, P. L., Waterhouse, R. & Itoh, T. (2011). Antenna miniaturization using slow wave enhancement factor from loaded transmission line models. *IEEE Transactions on Antennas and Propagation, 59*(1), 48-57.

4. Scardelletti, M. C., Ponchak, G. E., Merritt, S., Minor, J. S. & Zorman, C. A. (2008). Electrically small folded slot antenna utilizing capacitive loaded slot lines. In *IEEE Radio Wireless Symposium*, Orlando (pp. 731-734).

5. Liu, Q., Hall, P. S. & Borja, A. L. (2009). Efficiency of electrically small dipole antennas loaded with left-handed transmission line. *IEEE Transactions on Antennas and Propagation, 57*(10), 3009-3017.

6. Kamada, S., Michishita, N. & Yamada, Y. (2010). Short-length leaky wave antenna using composite right/left-handed ladder network for UHF band. In *International Workshop on Antenna Technology*, Lisbon(pp. 1-4).

7. Antoniades, M. A. & Eleftheriades, G. V. (2008). A folded-monopole model for electrically small NRI-TL metamaterial antennas. *IEEE Antennas Wireless Propagation Letters, 7*, 425-428.

8. Caekenberghe, K. V., Behdad, N., Brakora, K. M. & Sarabandi, K. (2008). A 2.45-GHz electrically small slot antenna. *IEEE Antennas Wireless Propagation Letters, 7*, 346-348.

9. Takahagi, K., Otsu, Y. & Sano, E. (2012). 2.45 GHz high-gain electrically small antenna with composite right/left-handed ladder structure. *IET Electronics Letters, 48*(16), 971-972.

10. Caloz, C. C., Sanada, A. & Itoh, T. (2004). A novel composite right-/left-handed coupled-line directional coupler with arbitrary coupling level and broad bandwidth. *IEEE Transactions on Microwave Theory and Techniques, 52*(3), 980-992.

11. Daly C. D. & Chandrakasan A. P. (2007). An energy-efficient OOK transceiver for wireless sensor networks. *IEEE Journal of Solid-State Circuits, 42*(5), 1003-1011.

12. Huang X., Harpe P., Wang X., Dolmans G., & Groot H. D. (2010). A 0dBm 10Mbps 2.4GHzultra-low power ASK/OOK transmitter with digital pulse-shaping. In *IEEE Radio Frequency Integrated Circuits Symposium*, Anaheim (pp. 263-265).

13. Mercier, P. P., Bandyopadhyay, S., Lysaght, C. A., Stankvoic, M. K. & Chandrakasan, P. A. (2014). A sub-nW 2.4 GHz Transmitter for Low Data-Rate Sensing Applications. *IEEE Journal of Solid-State Circuits, 49(7)*, 1463-1474.

14. Chee Y.H., Niknejad A.M. & Rabaey J. (2006). A 46% Efficient 0.8 dBm Transmitter for Wireless Sensor Network. *IEEE VLSI Symposium Digested of Technical Papers*, 43-44.

Figure captions

Table 1 Device sizes in the transmitter

Name	Size	Name	Size	Name	Size
M1	**W=3 μm**	**M7**	**W=4.5 μm**	**Ind. 1**	**W_{ind}=15 μm, R=116 μm, N_{ind}=5**
M2	W=12 μm	M8	W=75 μm	Ind. 2	W_{ind}=15 μm, R=109 μm, N_{ind}=3
M3	W=12 μm	M9	W=120 μm	Var. 1	W_{var}=2.5 μm, N_{var}=30
M4	W=3 μm	M10	W=32 μm	Var. 2	W_{var}=2.5 μm, N_{var}=30
M5	W=6 μm	M11	W=26 μm	Cap.	826 fF
M6	W=6 μm				

Table 2 Comparison of fabricated OOK transmitter with those measured in literature

Reference	CMOS technology	Frequency (GHz)	Power consumption (mW)	Output power (dBm)	With antenna
This work	180 nm	2.42	1.96	-6.8	yes
This work	180 nm	2.42	1.96	-4.6	no
[11]	180 nm	0.916	9.1	-2.2	no
[12]	90 nm	2.4	2.3	0	no
[13]	180 nm	2.48	0.191	>-29	yes
[14]	130 nm	1.9	1.35	0.8	yes

Electronic Supplementary Material for Analog Integrated Circuits and Signal Processing

Low-power, small-size transmitter module with metamaterial antenna

Kazuki Hiraishi*, Toshiki Wada*, Keishi Kubo*, Yutaro Otsu*, Masayuki Ikebe†, and Eiichi Sano*

*Research Center for Integrated Quantum Electronics, Hokkaido University, Sapporo 060–8628 Japan

†Graduate School of Information Science and Technology, Hokkaido University, Sapporo 060–0814 Japan

Tel: +81-11-706-7174, Fax: +81-11-706-6004

E-mail: esano@rciqe.hokudai.ac.jp

The effect of a connector nearby the antenna

Antenna characteristics could be affected by a connector nearby the antenna. We measured this effect by using two standard dipole antennas in an electromagnetic shield. The measurement setup is shown in Figure S1. Figure S2 shows the measured transmission between two antennas with and without a connector. The difference was less than 1dB. We concluded that the effect of a connector and cable nearby the antenna was negligibly small.

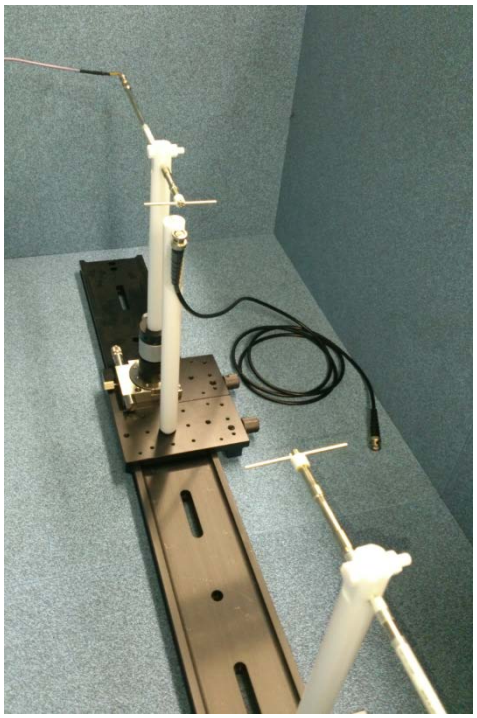

Figure S1 Measurement setup

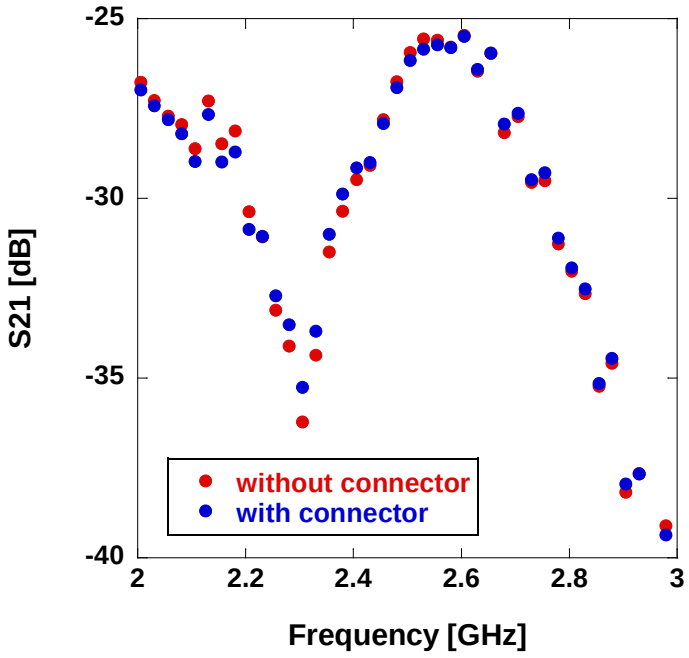

Figure S2 Measurement result

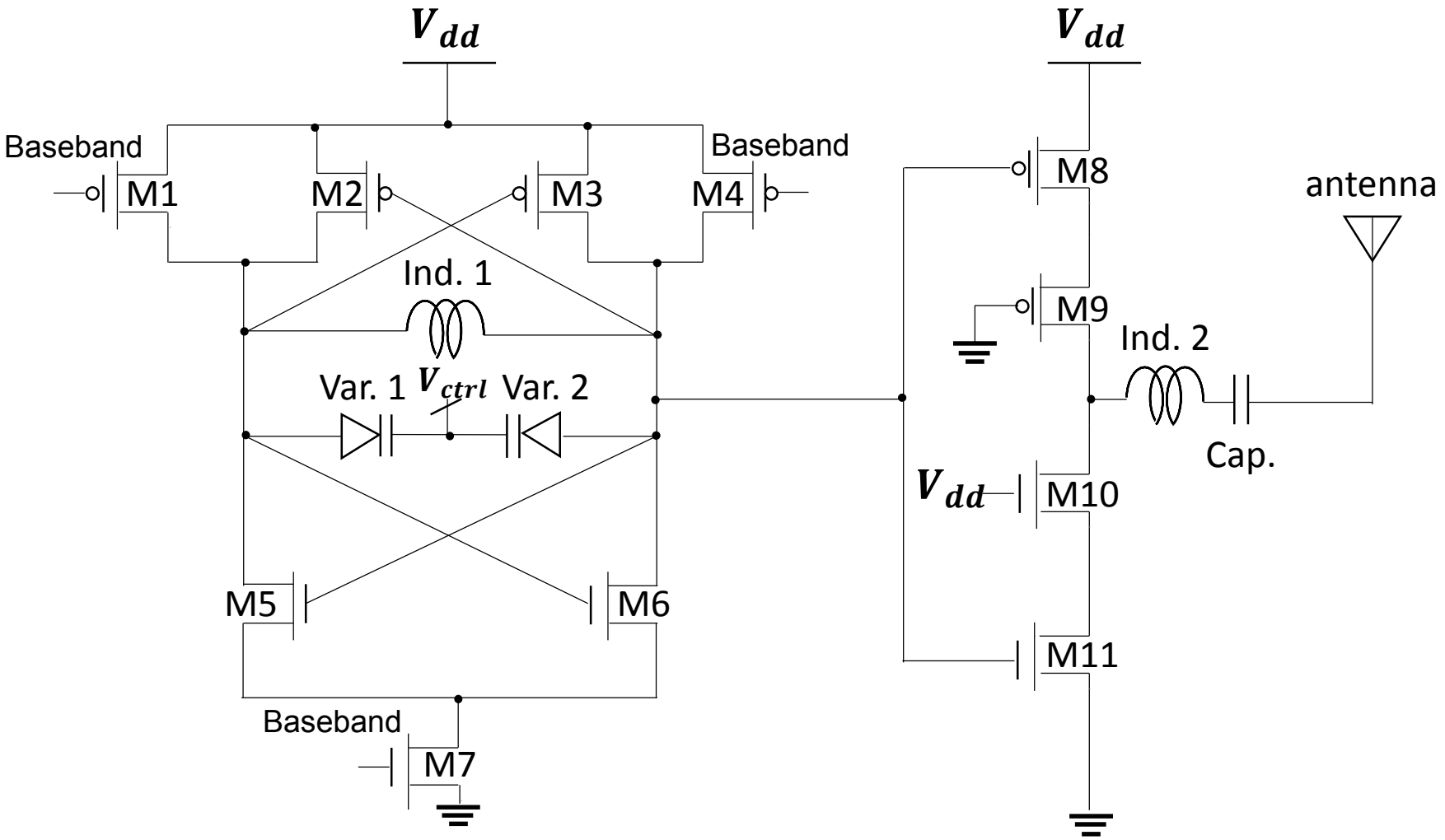
V_{dd}
V_{dd}
Baseband
M1
M2
M3
M4
Baseband
Ind. 1
Var. 1
V_{ctrl}
Var. 2
M5
M6
Baseband
M7
M8
M9
antenna
Ind. 2
Cap.
V_{dd}
M10
M11

Fig. 1

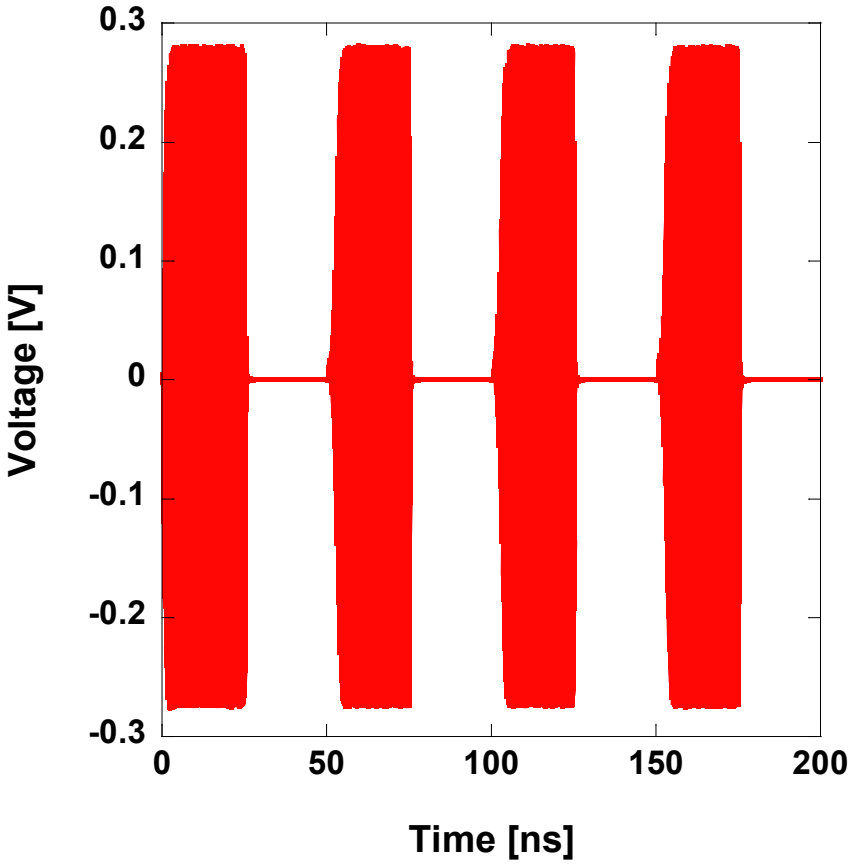

Fig. 2

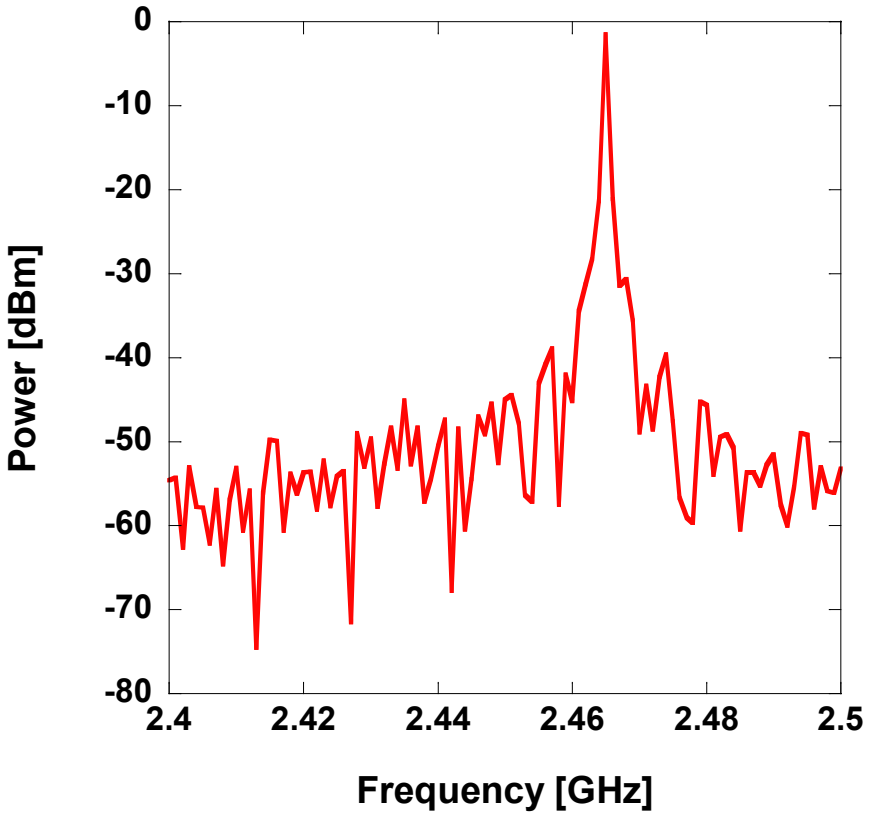
0
-10
-20
-30
-40
-50
-60
-70
-80
Power [dBm]
2.4
2.42
2.44
2.46
2.48
2.5
Frequency [GHz]

Fig. 3

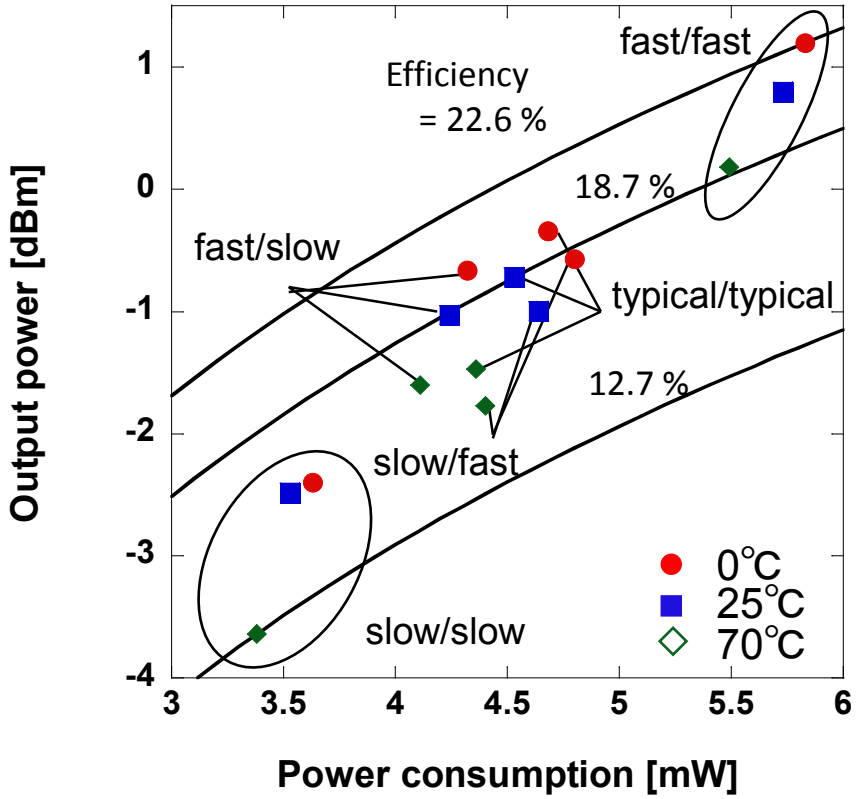
Output power [dBm]
Power consumption [mW]
1
0
-1
-2
-3
-4
3
3.5
4
4.5
5
5.5
6
Efficiency
= 22.6 %
18.7 %
12.7 %
fast/fast
fast/slow
typical/typical
slow/fast
slow/slow
0℃
25℃
70℃

Fig. 4

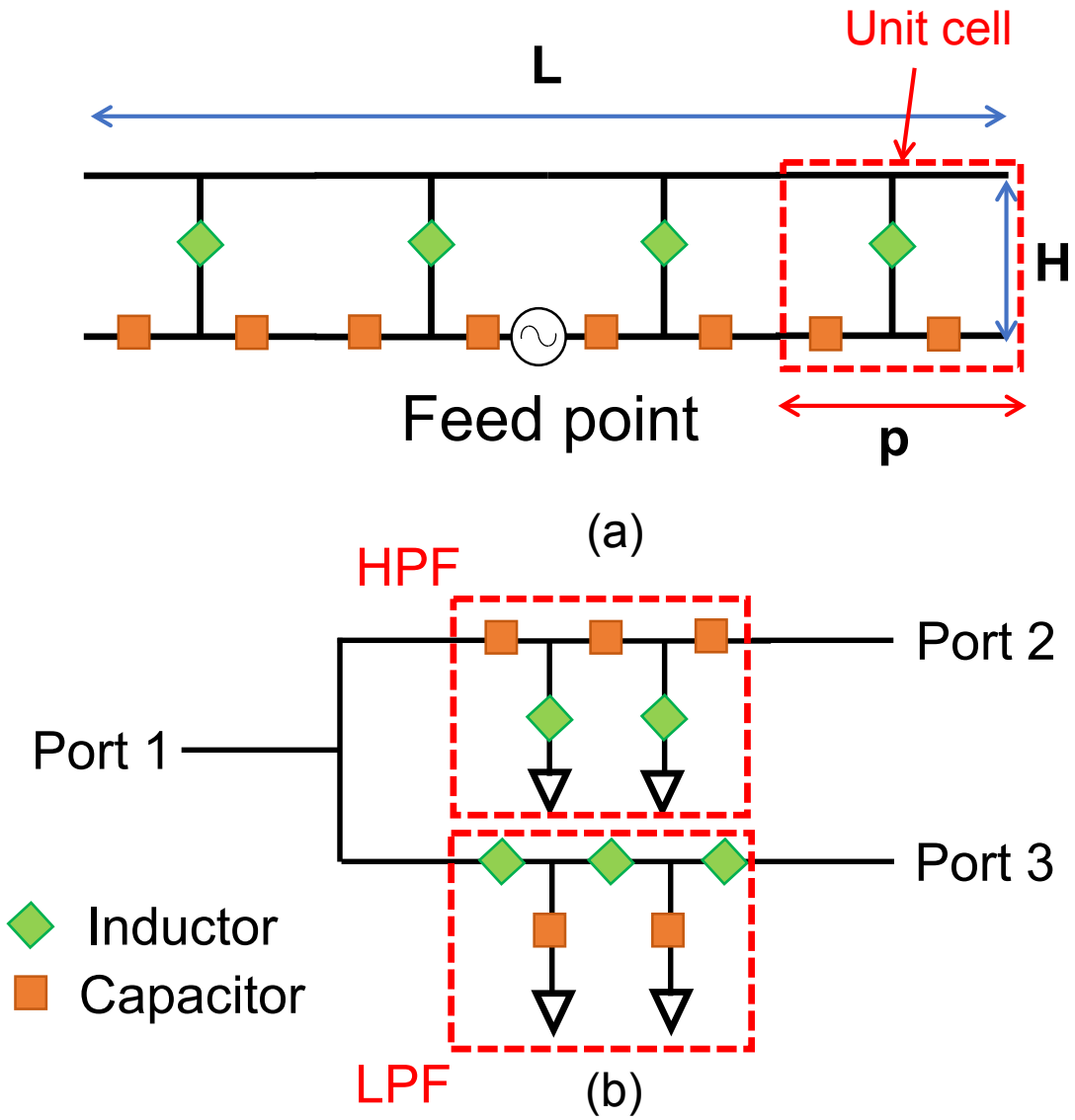
Unit cell
L
H
Feed point
p
(a)
HPF
Port 2
Port 1
Port 3
Inductor
Capacitor
LPF
(b)

Fig. 5

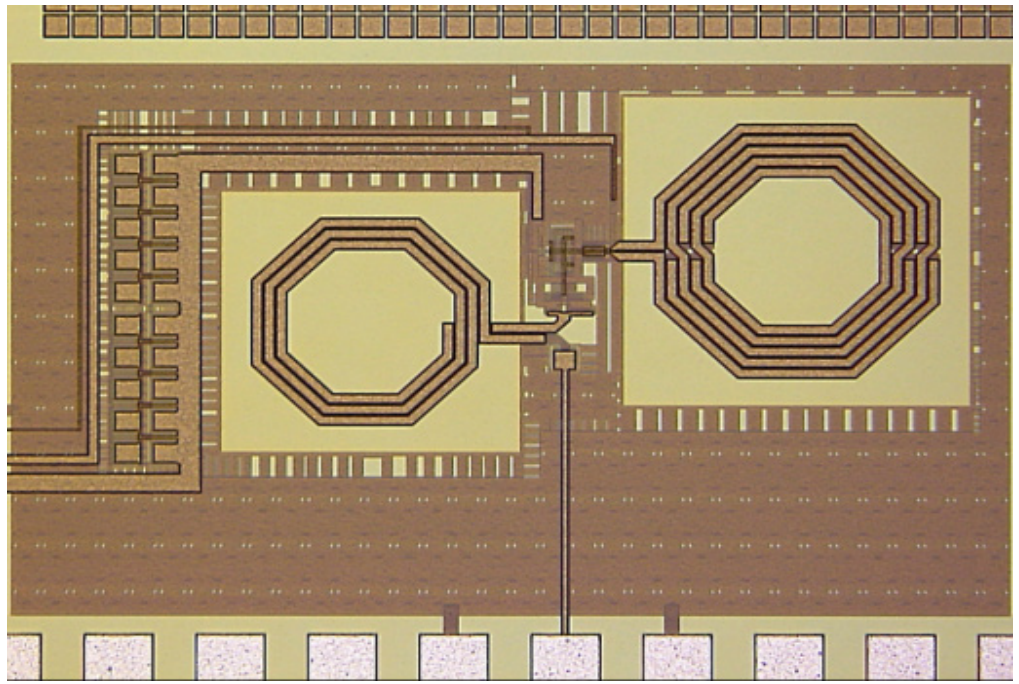

Fig. 6

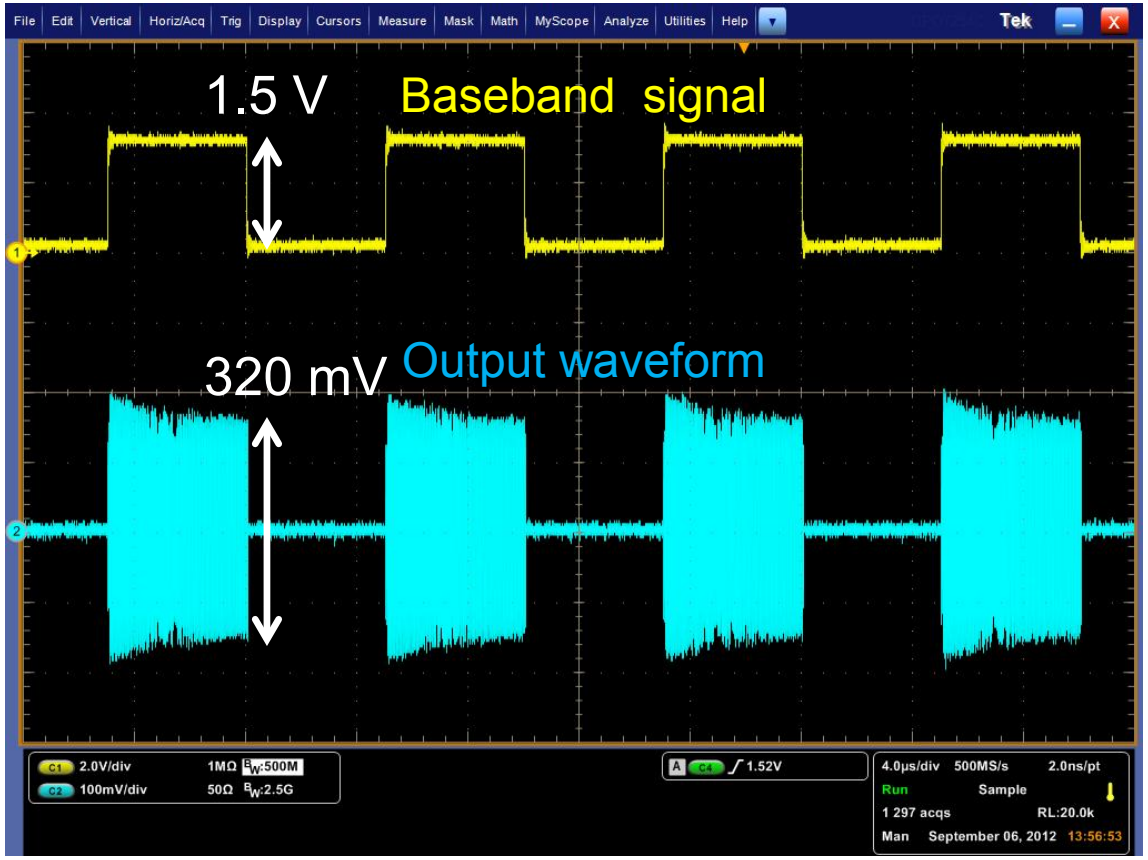
File
Edit
Vertical
Horiz/Acq
Trig
Display
Cursors
Measure
Mask
Math
MyScope
Analyze
Utilities
Help
Tek
1.5 V
Baseband signal
320 mV
Output waveform
C1 2.0V/div
1MΩ BW:500M
C2 100mV/div
50Ω BW:2.5G
A C4 1.52V
4.0µs/div 500MS/s 2.0ns/pt
Run Sample
1 297 acqs RL:20.0k
Man September 06, 2012 13:56:53

Fig. 7

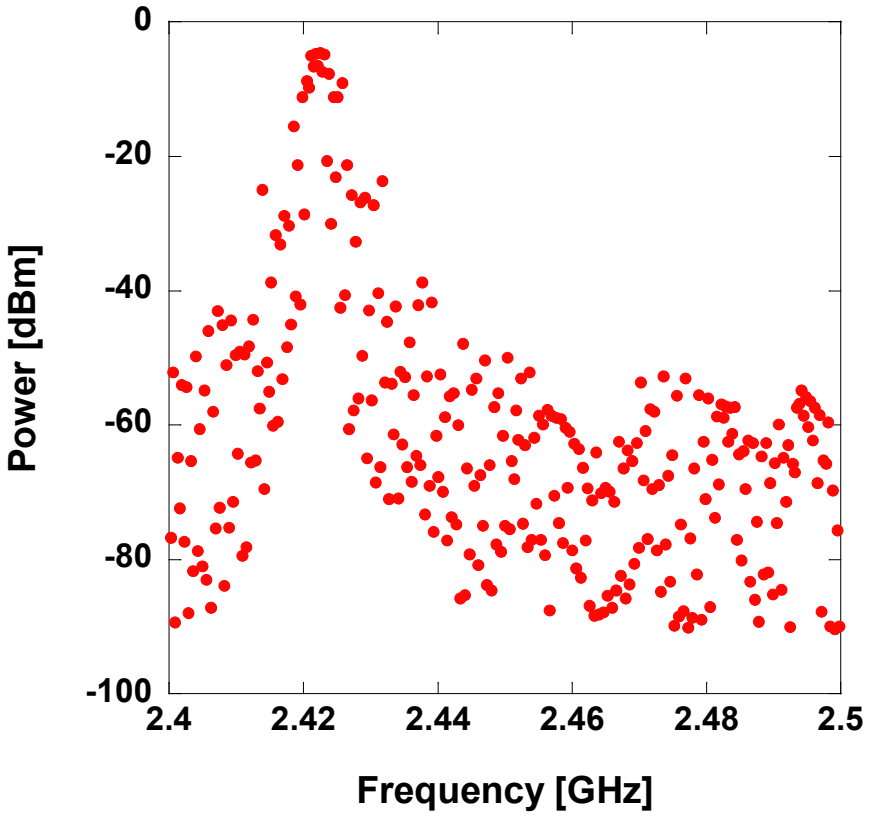

Fig. 8

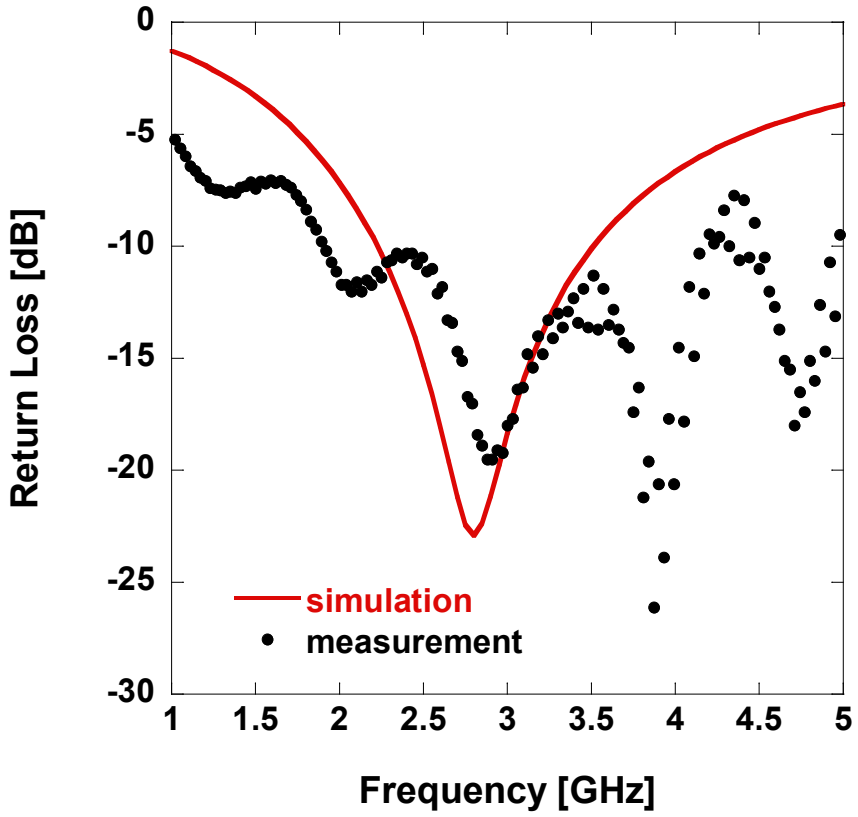
0
-5
-10
-15
-20
-25
-30
Return Loss [dB]
1
1.5
2
2.5
3
3.5
4
4.5
5
Frequency [GHz]
simulation
measurement

Fig. 9

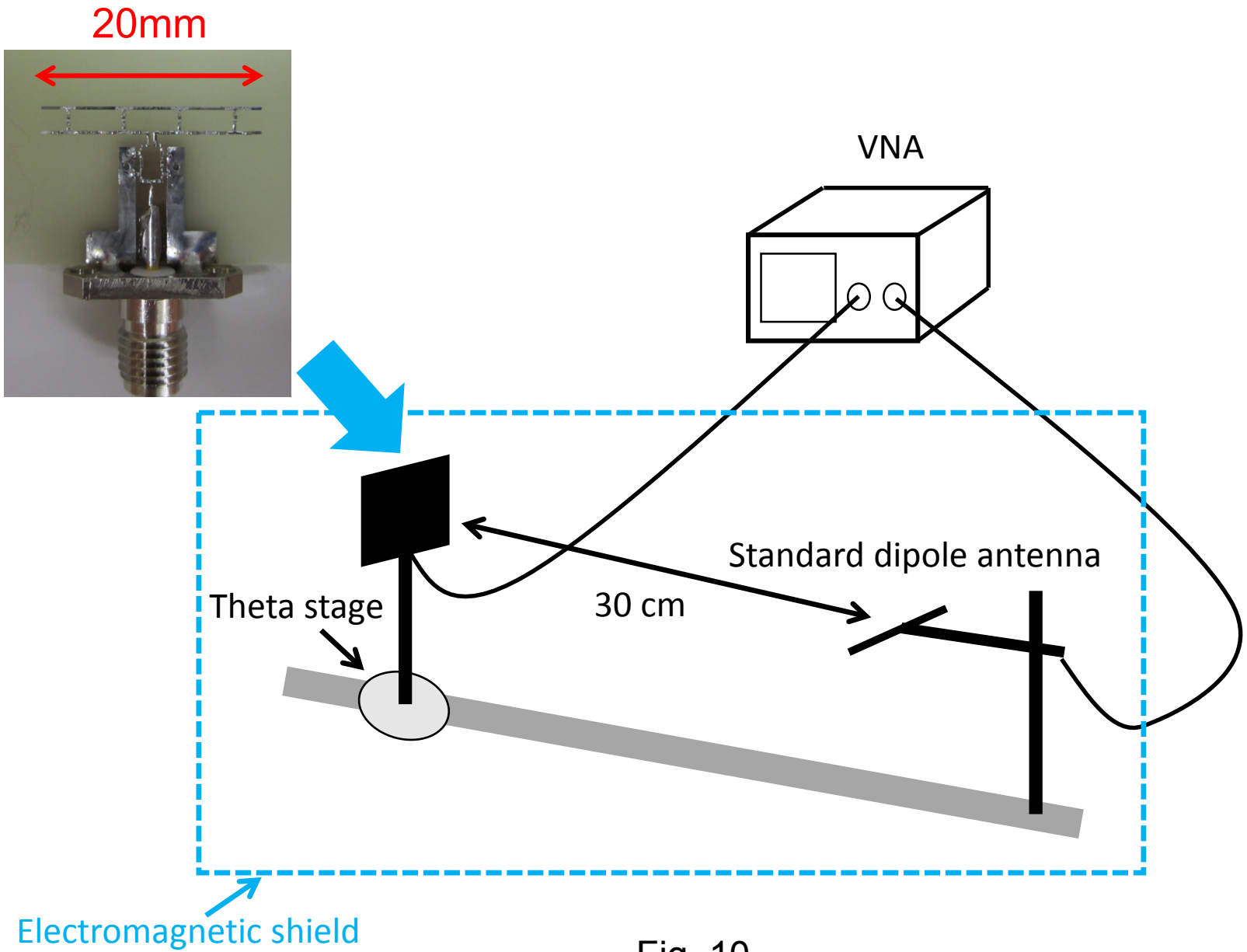
20mm
VNA
Standard dipole antenna
30 cm
Theta stage
Electromagnetic shield

Fig. 10

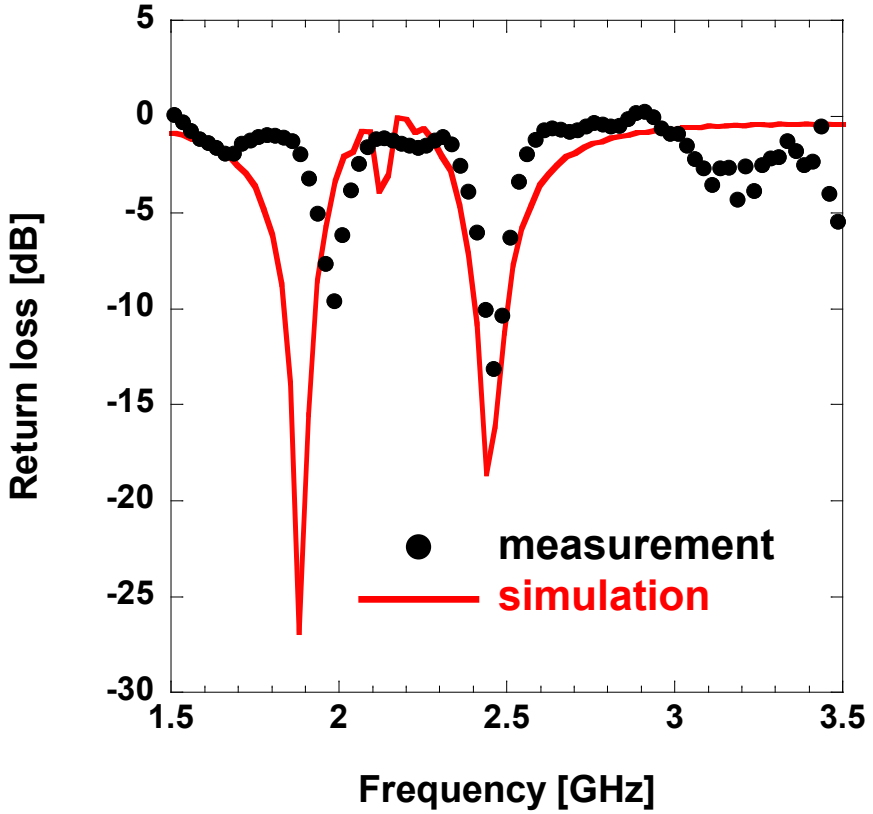
5
0
-5
-10
-15
-20
-25
-30
Return loss [dB]
1.5
2
2.5
3
3.5
Frequency [GHz]
measurement
simulation

Fig. 11

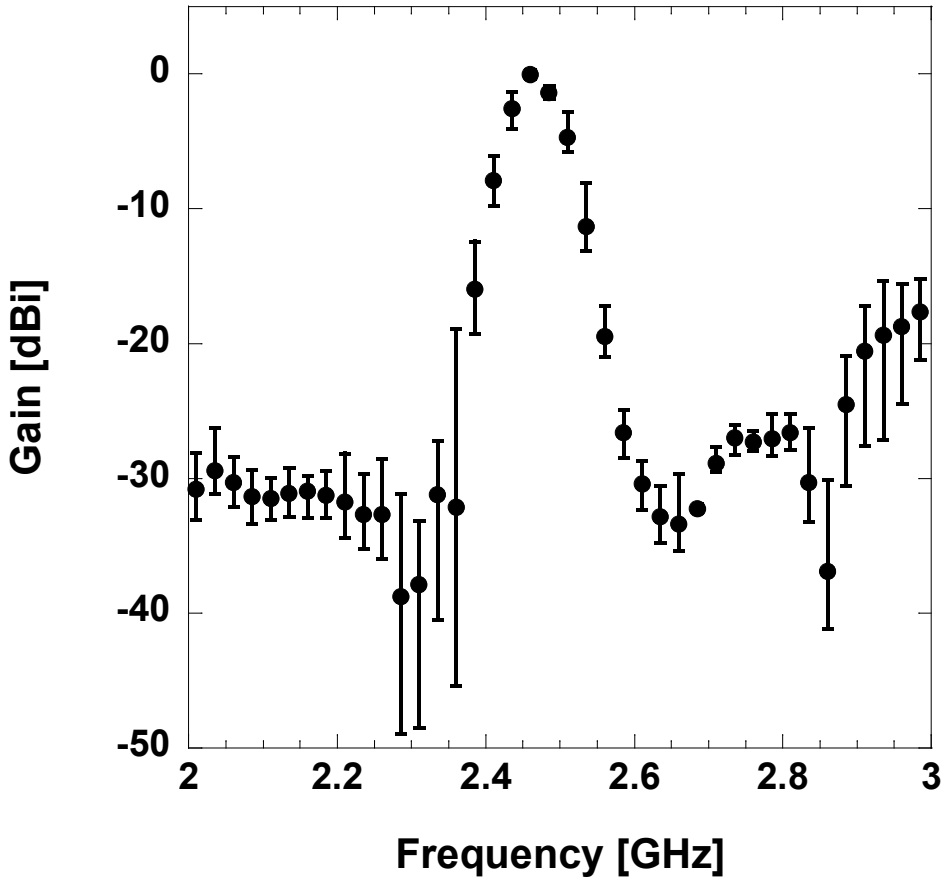

Fig. 12

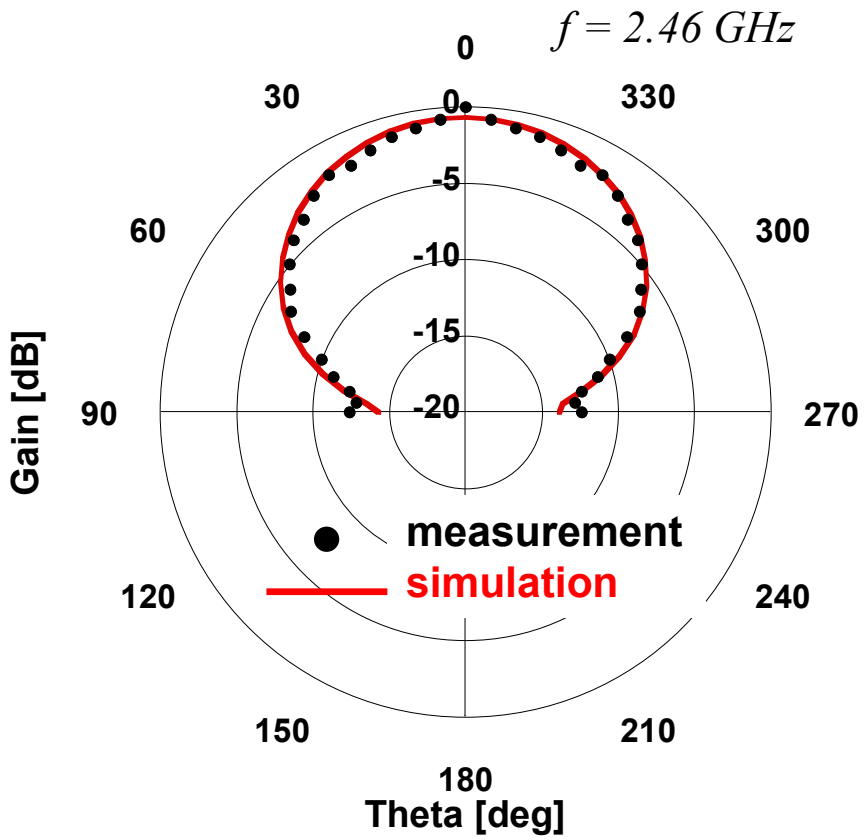
f = 2.46 GHz
0
30
330
60
300
90
270
120
240
150
210
180
0
-5
-10
-15
-20
Gain [dB]
Theta [deg]
measurement
simulation

Fig. 13

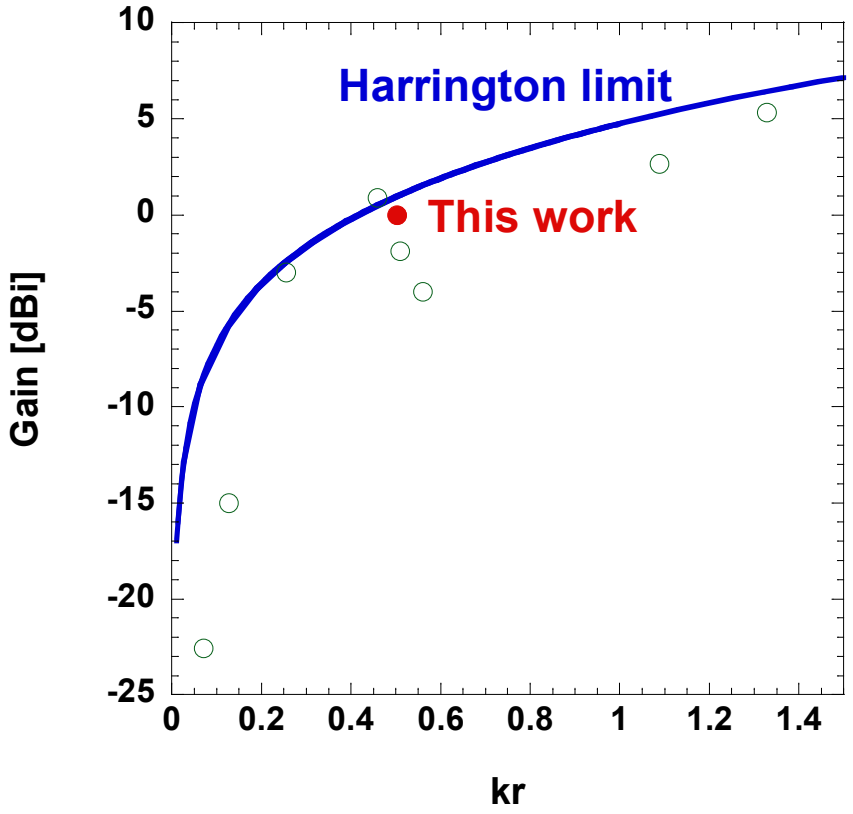
Harrington limit
This work
Gain [dBi]
kr
10
5
0
-5
-10
-15
-20
-25
0
0.2
0.4
0.6
0.8
1
1.2
1.4

Fig. 14

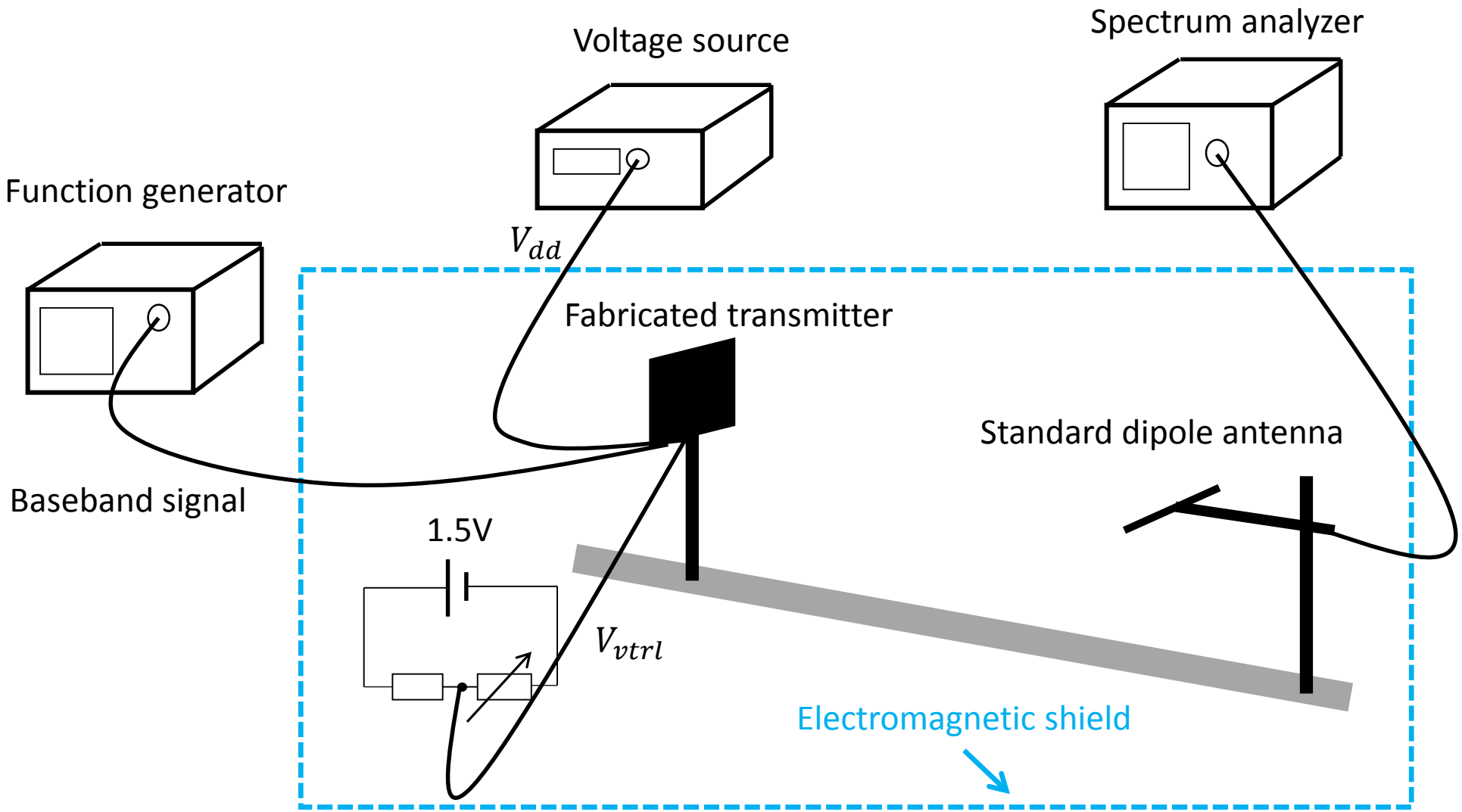
Voltage source
Spectrum analyzer
Function generator
V_{dd}
Fabricated transmitter
Standard dipole antenna
Baseband signal
1.5V
V_{vtrl}
Electromagnetic shield

Fig. 15

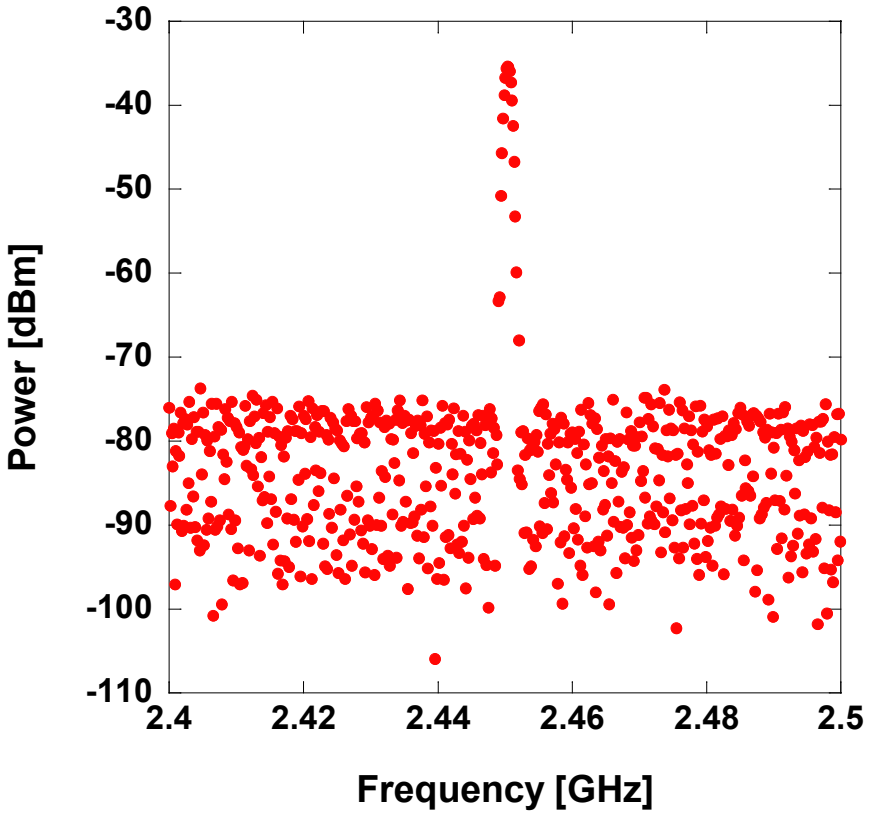
-30
-40
-50
-60
-70
-80
-90
-100
-110
Power [dBm]
2.4
2.42
2.44
2.46
2.48
2.5
Frequency [GHz]

Fig. 16

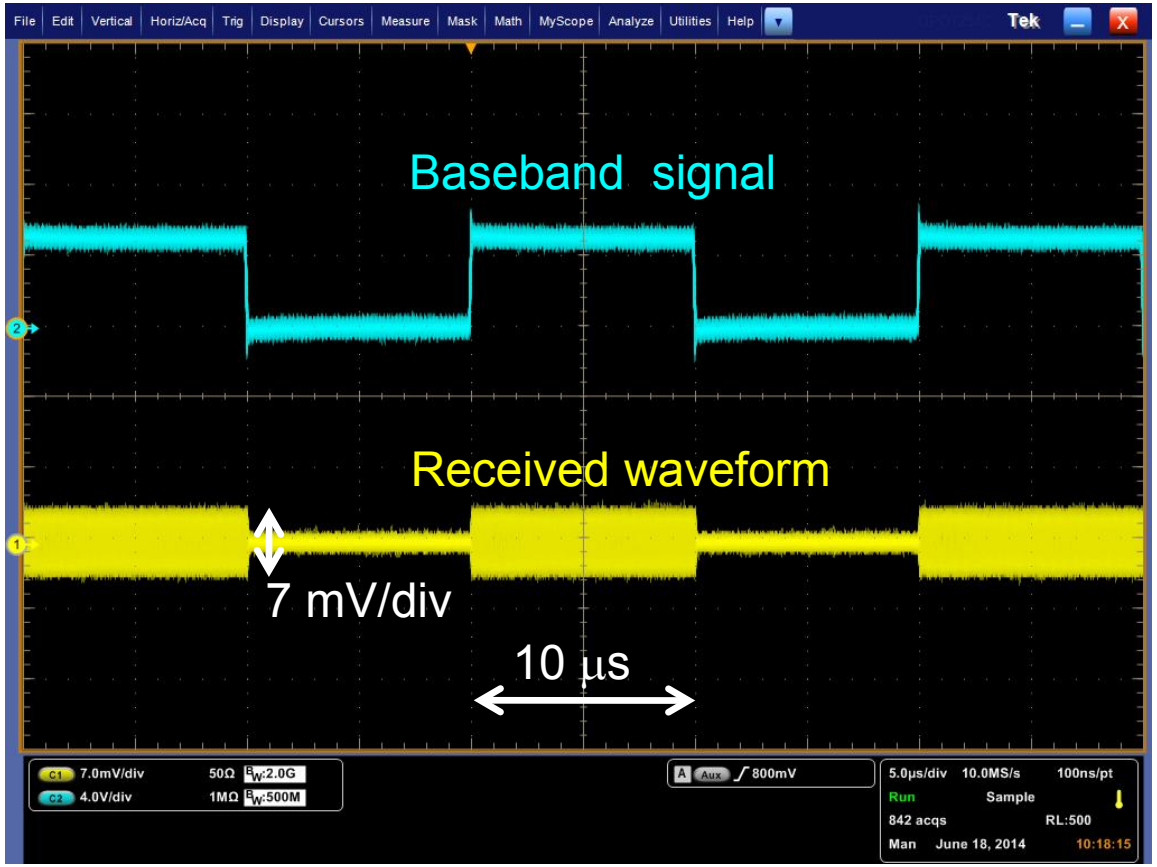
File Edit Vertical Horiz/Acq Trig Display Cursors Measure Mask Math MyScope Analyze Utilities Help
Tek
Baseband signal
Received waveform
7 mV/div
10 µs
C1 7.0mV/div 50Ω BW:2.0G
C2 4.0V/div 1MΩ BW:500M
A Aux 800mV
5.0µs/div 10.0MS/s 100ns/pt
Run Sample
842 acqs RL:500
Man June 18, 2014 10:18:15

Fig. 17